Strengthening the bridge between academia and operations for orbital debris risk mitigation

Mark A. Vincent
Raytheon

ABSTRACT

The benefits of using Keplerian or equinoctial elements throughout the end-to-end process from doing orbit determination to the calculation of the Probability of Collision (Pc) are investigated. Additional topics include an update and new application of a previously published tool for Pc forecasting, and a discussion of using Monte Carlo as a standard for probabilistic analysis.

1. INTRODUCTION

This paper and the previous two papers by the same author [1,2] have the common theme of attempting to match the analysis done by the academic community with needs of the operational teams doing risk mitigation from orbital debris (and active satellites) for their missions. Although a lot of progress has been made, the operators are still struggling to maintain their acceptable risk without overtaxing the personnel involved. In this vein, several teams are adding automations to their processes, in particular in anticipation of an increase of three to ten times more conjunctions to consider when the Space Fence becomes operational.

Lately, academia seems to have focused on the following three areas:

a) Covariance propagations
b) Testing of covariance realism
c) Expanding 3-D calculations of Probability of Collision (Pc) to high speed conjunctions

The identification, tracking and cataloging of objects will be delegated a set of separate topics not directly addressed in this paper. However, the Orbit Determination (OD) directly related to a) and b) will be discussed. The first topic of this paper investigates expanded use of Mean equinoctial elements in the process to calculate Pc and thus has ties to a), b) and c) as well as OD. A critique of b) will be included in a subsequent paper.

2. CALCULATING Pc WITH EQUINOCTUAL ELEMENTS

The motivation for this topic comes from watching the evolution of conjunction parameters, in particular the radial component of the combined (primary and secondary) covariance in real-life conjunctions. Admittedly navigating the Orbit Carbon Observatory 2 (OCO-2) which has GPS- tracking biases one to have expectations of a “well-tracked primary.” And following the distinction of Sabol [3], in general “catalogued” objects, corresponding to at least two sets of tracking data, will be considered here, as opposed to single-tracked secondaries. Fundamentally this means that the uncertainty in the semi-major axis (sma), either Mean or Osculating, of the primary will be in meters (or less) to 10’s of meters and for the secondary 10’s (or less) to 100’s of meters. Note that when discussing Mean sma, it is also assumed that the conversion back and forth from Osculating sma can be done at 10 m or less, a subject that will discussed a bit later.

Of course, when comparing radial uncertainties to sma uncertainties the eccentricity vector uncertainties of the two orbit is a significant factor. An extreme and interesting example of this was illustrated [4] when OCO-2 had repeated conjunctions with the same object over a dozen times in August 2016. In this case the secondary had a sma about 3 km less than OCO-2 but the eccentricity of only twice that of OCO-2 was enough to make the orbits cross. And the repeating nature was caused by nodal precession rates of opposite signs that dominated the effect of the difference in mean motions for the total encounter period of almost a day. As explained in the following, using Keplerian or equinoctial elements might reduce the number of elements whose uncertainties are relevant from six to five for the calculation of Pc.

The new proposed approach to calculating Pc has strong analogies to the "close approach" methodology. The three filters suggested by Hoots [5] and further discussed by Woodburn [6] are a good framework for this discussion. The first one, the apogee/perigee filter, is usually considered a binary process (either a close approach occurs or it doesn't). However, the uncertainties involved are a good segue to the first step of the new approach. Furthermore, the filter provides an example of how osculating effects can confuse the process. Consider the reference orbit for the Earth Science Constellations (ESC) comprised of the A-Train that contains OCO-2 and the Morning Constellation. The reference orbit is sun-synchronous and has a groundtrack that repeats in 16 days and 233 revolutions. It has a frozen eccentricity vector corresponding to a Mean eccentricity value of 0.00118 and a Mean argument of perigee (ω) of 90 degrees.

Define "Index Height" (IH) as a radial value minus the Earth's equatorial radius (R_E). The middle solid line in Fig. 1 is the actual index height during one orbit revolution (the second figure of [6] is analogous for multiple orbits and using radius rather than index height). At the nodes the index height is about 705 km and hence the ESC constellation are said to be in "705-km orbits." Osculating "apogee" and "perigee," values can be defined by a* (1+/- e) - R_E where a and e are the instantaneous osculating semi-major axis and eccentricity and are the top and bottom solid lines respectively. Thus the first interesting observation is that the minimum height occurs at an osculating apogee rather than an osculating perigee (this occurs in all cases with the 45 < Mean ω < 135 degrees or 225 < Mean ω < 315 degrees; when Mean ω = 45, 135, 225 or 315 degrees the Osculating e is close to zero at the minimum IE, thus the perigee is both an osculating "apogee" and "perigee").

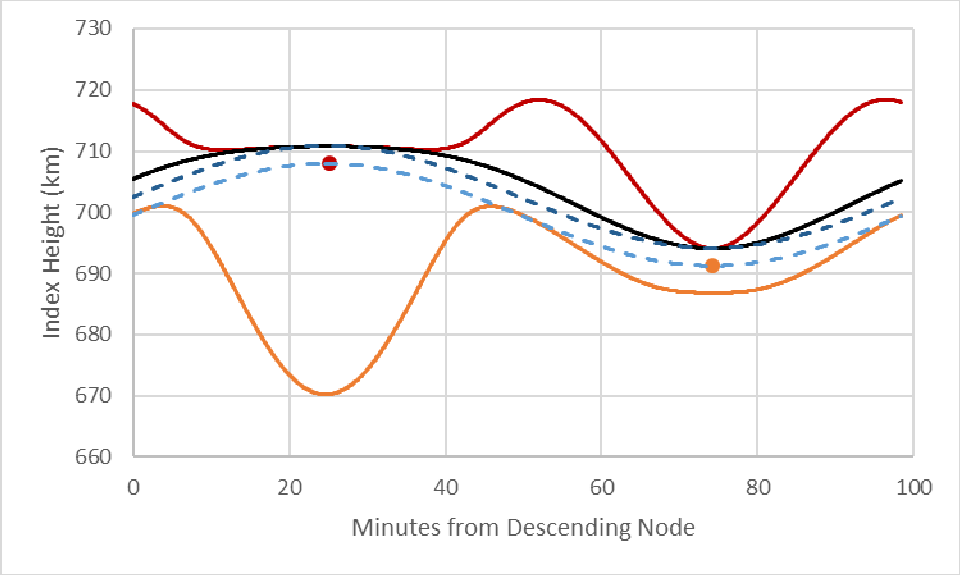

Fig. 1. Apogee and Perigee and Mean and Actual Index Heights

The corresponding unperturbed two-body orbit represented by Mean elements is shown in the lower dashed line, with a Mean semi-major axis of 7077.723 km. The two dots represent the apogee and perigee for that orbit. Note they are almost 3 km below the actual IE maximum/minimum and thus problematic for either close approach (as pointed out in [6]) or Pc calculations. Note the difference near the poles between actual and Mean is closer to 5 km which leads to organizations like the European Space Agency classifying the ESC as 700 km orbits (i.e. index height of 7077.732 – 6378.137 km), as opposed to the NASA 705 km definition mentioned previously.

However, as discussed on Page 285 of [7] and Page 870 of [8] the secular effects of the dominant J_2 term of the gravity field can be used to create new "Mean" values. In particular, the new Mean mean motion is:

$$n' = n_0 \left[1 + \frac{3}{2}\frac{J_2 R_E^2}{p^2}\left(1 - \frac{3}{2}sin^2(i)\right)(1-e^2)^{1/2}\right] \quad (1)$$

With p = $a_0(1\text{-}e_0^2)$ and i being the orbit inclination. As pointed out in [8] the new nodal period is not 2π times the inverse of n' because, in general the argument of perigee also has a secular motion. Taking that into account the new nodal period is:

$$P' = P_0 \left[1 - \frac{3}{2} \frac{J_2 R_E^2}{p^2} (3 - 4 \sin^2(i))(1 - e^2)^{1/2}\right] \quad (2)$$

Also note this is an example of the new frequencies introduced in Kolmogrov, Arnold and Moser (KAM) theory discussed in [9]. In [7], Roy suggests a new Mean semi-major axis, however when it is cubed and multiplied by the square of the n' above it does not equal the gravitational parameter μ. So instead, choose the new value of *a'* to be:

$$a' = a_0 \left[1 - \frac{J_2 R_E^2}{p^2} (1 - \frac{3}{2} \sin^2(i))(1 - e^2)^{1/2}\right] \quad (3)$$

which now does satisfy the normal version of Kepler's third law when used with n' (to the consistent order in J_2). Also if this new *a*' is used along with the appropriate true anomaly corresponding to n' to calculate the radius value, a new index height is produced which is shown by the upper dashed line in Fig. 1. It matches the true and osculating values at the maximum/minimum index height quite well. However, higher order effects cause a difference of around a 100 m, so these new Mean values might be okay in a "padded" [5] close approach analysis but they would still not be suited for Pc calculations where 10 m, if not better, radial accuracy is needed.

A historical anecdote on the apogee/perigee issue addresses the longer term effect of the secular and long-term motions on the Mean elements. The ESC teams were interested in defining which missions could never collide with them, in particular for new missions joining or old missions exiting the constellations. The old rule used the 711 apogee and 694 km perigee values (the maximum/minimum index heights of Fig. 1) and added a 2 km margin. That is, a satellite below was compliant when its apogee value was less than 692 km. However as presented in [10] and [11], the maximum Mean eccentricity value occurs when the Mean argument of perigee is 90 degrees (i.e. the frozen value). Even if the Mean argument of perigee of the secondary orbit evolves to 270 degrees due to the long-term effects, the minimum separation of the orbit remains the same to first order:

$$\Delta r = | \Delta a | - | a_s * \Delta e | \quad (4)$$

where a_s is the semi-major axis of the secondary and Δe represents the magnitude that the secondary's eccentricity vector is different than the frozen value [11]. This led to the approval of a new 'Constellations Envelope" that is an ellipsoidal +/- 2 km shell around the ESC reference orbit at all longitudes.

Before presenting the new approach and its analogies to the second and third close approach screening methods, a further discussion on Mean elements is warranted. Vallado gives an extensive review of Mean element theories. In particular, he describes the Draper Semianalytical Satellite Theory (DSST) which in the following discussion will be assumed to be the basis for doing orbit determination with equinoctial elements [12, 13]. Vallado does mention Kwok's J_2 theory but omits the follow-on work that was performed at the Jet Propulsion Laboratory. Kwok's program was extended to the full gravity field including J_2-squared and called the Long-term Orbit propagator (LOP) which later became the POLOP and then later part of POPS (Planetary Observer Planning Software) [14]. With the inclusion of higher order gravity terms a program was needed to convert back and forth between Mean and Osculating elements with the same theory. Guinn [15] created a program named OSMEAN to do this using Kaula's formulation [16] (and was used in the conversions inherent in Fig.1). Later Ely created another JPL tool named Morbiter which did the conversions numerically [17] and was closer to the DSST formulation (and also does the semianalytical propagation [18] of POLOP and DSST).

How much of the short-period variations that are taken out is the relevant topic when comparing all the different conversion Mean/Osculating conversion tools. For example, older theories such as Brouwer-Lydanne and Kozai-Itsak leave variations of 100's of meters in the Mean semi-major axis, and the former does not work for the eccentricity vector components beyond J_2. The more modern theories work much better, OSMEAN produces Mean semi-major axis variations of just under 10 meters and Morbiter and DSST are slightly better. Obviously if Mean elements are to be used in Pc calculations, not only does the process have to be consistent but the conversions will likely have to be with one of the modern methods of removing/adding the short-period terms.

The Proposed New Approach

Dividing the process into three stages: orbit determination (OD), propagation of state and covariance and calculation of Pc, it will be assumed that the OD has been done in equinoctial elements ala DSST and those elements have been propagated to the time of closest approach (TCA) via a state transition without incurring significant errors. This latter subject has been the focus of a lot research. Here we will assume that fourth and fifth figures of [19] apply. That is, the non-linear aspects do make propagating equinoctial elements better than using Cartesian and when using equinoctial and the reasonably sized semi-major axis errors discussed above, the non-linearity is not a factor for the 5 days (around 75 orbits) maximum time period of interest in the Pc calculation process. Though it should be acknowledged that the difference between such methods as KRATOS [20] that use a mixture of Cartesian and "J_2 equinoctial" elements versus using similar equinoctial elements throughout is not clear without more analysis.

The new approach will be divided into two parts, whether the orbits of the primary and secondary are intersecting and then, if they are intersecting, whether both are at the one of two intersecting points at the same time. Thus the first step is analogous to the Geometric Filter of Hoots [4] (called the Orbit Path filter by Woodburn [5]) and the second step is similar to the Timing Filter of both authors. Satisfying both spatial and temporal intersection conditions (hereafter called SIC and TIC) is called by Woodburn as being "at the right place at the right time" though it seems more appropriate to state it as being "at the wrong place at the wrong time." Another important, though somewhat obvious, observation is that if the probability of the orbits intersecting is known to be less than the threshold of interest, then the second step is not even necessary. This importance is further emphasized by TIC containing the fast variable, true anomaly or its equivalent, while the SIC does not.

First develop the problem in terms of Keplerian/equinoctial elements without including the uncertainties. The relative line of nodes representing the line of intersection between the two orbit planes (Fig. 2) is a vector formed by the two respective angular momentum vectors. Call this vector $\vec{I}$ and its magnitude I, then in terms of the angular momenta:

$$\vec{I} = \vec{h}_1 \times \vec{h}_2 \qquad I = h_1 h_2 \sin(\theta) \qquad \cos(\theta) = \vec{h}_1 \bullet \vec{h}_2 / h_1 h_2 \tag{5}$$

noting that that the angular momenta quantities can be calculated directly from the equinoctial elements assumed here to be products of the orbit determination/propagation (the Keplerian equivalent is shown on the next page).

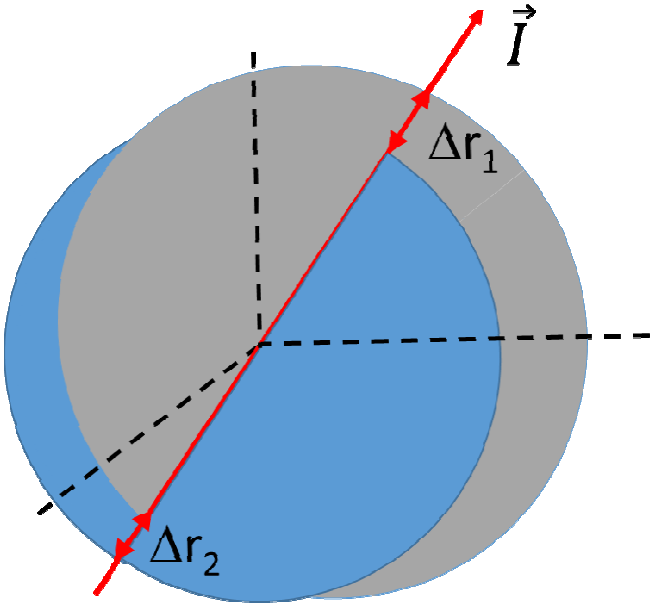

Fig. 2. Geometry along the Intersection Line of the Orbit Planes

One argument of latitude for each orbit at the line of intersection can be derived from the dot product of $\vec{I}$ and the corresponding orbit's ascending node vector. For each orbit, the second argument of latitude is 180 degrees greater. Subtracting the corresponding argument of perigee for each orbit gives a pair of true anomalies for that orbit corresponding to the two potential intersection points. To simplify the discussion and notation, hereafter only one potential intersection point will be considered. That is, only consider the conjunction in the northern hemisphere (or some similar designation if one of the orbits is equatorial), but realize in reality there will be two conjunctions to consider. Up to this point the two orbit planes have been assumed to be not co-planar. As pointed out in [5] the closest approach in general does not have to be at the line of intersection. So for this discussion the requirement will be that the orbits planes are not even close to being co-planar. A rigorous definition of what "close' means is warranted. But in the interim, consider enough angular separation of the orbit planes such that the distance along either orbit away from the intersection line before the separation between the planes equals the combined Hard Body Radius (HBR) of the two objects is small compared to the uncertainties involved in the SIC.

Let r_1 and r_2 be the radial values for first and second orbits at the intersection line for this conjunction, they come simply from the two-body formula:

$$r_1 = \frac{a_1\,(1 - e_1{}^2)}{1 + e_1\,\cos(\nu_1)} \qquad r_2 = \frac{a_2\,(1 - e_2{}^2)}{1 + e_2\,\cos(\nu_2)} \tag{6}$$

then similar to the close approach analysis, collision can only occur if $| r_2 - r_1 |$ is less than the combined HBR, again independent of where the objects are in their orbits. Up to this point the same equations apply, whether it is the two-body equations modeling the two-body situation (albeit with the angular momentum constant) or the instantaneous ellipses represented by the osculating elements in the full-gravity situation. However, they don't apply to the Mean elements (or the J_2 modified Mean elements presented above) of the full gravity situation. Specifically, the difference of the two Mean radii being within a chosen range does not guarantee that the difference of osculating (true) radii is in the same range.

To confirm this assertion numerically, the Mean elements of the ESC reference orbit were chosen with two different longitudes of ascending nodes so an ascending path crossed a descending path near 45 degrees of latitude (specifically the two orbits had true anomalies of +/- 45 degrees about the frozen argument of perigee of 90 degrees). Both sets of elements were converted to Osculating (50x50 gravity field) and then the whole process was iterated to the actual crossover point was achieved in Osculating elements. The final crossing geodetic latitude ended up at 44.420 degrees. The radius of both orbits was calculated and the descending path was 123.9 m higher. Again, this was for the "same orbit,' comparing two orbits in general could give even larger separation values. Stated otherwise, one cannot assume that the osculating effect on two satellites over the same point on the Earth is the same. This numerical test could have also been done analytically. For example, the linear solutions (Equation 3.76 in Kaula [16]) contain the term $S_{\ell mpq}$ which, as given by his Equation 3.71, includes a dependence on mean anomaly and longitude of ascending node (i.e. the values that were different for the two orbits in the numerical test).

Even though the osculating radii difference has to be ultimately used, the uncertainties involved can be divided into uncertainties in the Mean elements, errors in the conversion to Osculating elements and the indirect variation of Osculating elements due to variations in Mean elements. The last term is associated with the partial derivative B_1 in 5th equation of [12] and 3rd equation of [13]. They will be assumed to be known and the previously discussed errors in Mean to osculating conversion will be assumed to be small by using a good conversion method. Thus the remainder of the discussion will be on the Mean element uncertainties.

The angular momenta can be derived from the Keplerian elements via:

$$h^2 = \mu * a(1-e^2) \quad h_z = h\cos(i) \quad h_x = h\sin(i) * \sin(\Omega) \quad h_y = -h\sin(i) * \cos(\Omega) \tag{7}$$

noting that the last two equations have fixed signs while Equations 4.120 and 4.121 of [7] unnecessarily include +/- and -/+, at least for the usual convention of inclination ranging from 0 to 180 degrees. Also the third equation in [5] mistakenly has a "+" for h_y, though the subsequent equations are correct. So the uncertainty in angular momenta magnitude components depend directly on the uncertainties in a, e, i and Ω. Indirectly the secularly precessing value of Ω will depend on the uncertainties in a, e and i, again noting that this precession was very important in the geometry of the repeated conjunctions studied in [4]. Also note the osculating behavior of the angular momentum

both in magnitude and direction comes directly from the short periodic effects on a, e, i and Ω. Finally note that using Delaunay elements is even simpler since h and h_z are already present.

Turning to the equations for the radii, beside the already considered uncertainties in a and e, there is the added uncertainty in the true anomaly ν. At first this might be associated with the "fast' along-track variables, but it should be remembered that this is the ν from the perigee line to the intersection line, not the true anomaly (and associated along-track uncertainty) of the satellites itself. Therefore, the relevant uncertainty here should be associated with the uncertainty in the argument of perigee (ω), and the previously described uncertainty of the direction of the intersection line. Note that there is an interesting continuation of these derivations in [5] and they will be incorporated into future analysis.

In summary, the uncertainties for the spatial intersection condition is only dependent upon the "slow variables" a, e, i, Ω and ω. The importance of this will be discussed later, but note the latter four variables are minimally affected by uncertainties in solar flux and atmospheric drag (with an exception for highly elliptic orbits whose shape is highly affected by the drag at perigee). The Mean semi-major axes, a_1 and a_2, are affected by these drag effects in a correlated manner. If the secondary object has a ballistic coefficient similar to an intact satellite and both are in reasonably close to circular LEO orbits, then the differential effect caused by changes in drag will be relatively small (a few meters/day for A-Train altitude) compared to the radius differences of interest. However, in other cases the effect of drag could be over 10 times greater for the secondary. Then this differential effect will be important thought still be less than the indirect effect in the along-track direction caused by the semi-major axis difference.

In the case of the probability of spatial intersection being over the Pc threshold of interest, the next step is to look at the temporal intersection criteria. Keep in mind that if the threshold is $1x10^{-4}$ and the probability of the radial difference being less than the HBR is $1x10^{-3}$, then arguably the probability of the temporal intersection only has to be less than 10%, if the correlations between the two criteria are ignored. However, since the premise here is that a conjunction has been predicted by an initial screening with an associated TCA, it is already known that each object will cross the other object's orbital plane in a relatively small time interval that contains TCA. This where the similarities to both the two and three dimensional methods of calculating Pc become evident. The sensitivity was also evident in the repeated conjunctions of [4] since over the course of the conjunctions, first the primary (OCO-2), then the secondary and then finally the primary was reaching the other object's orbit plane first. The 5th column of Table 1 is the time the Object crossed OCO-2 orbit plane with respect to TCA and the 6th column is *vice versa*.

Table 1. Geometry and Timing of Repeated Conjunctions between OCO-2 and Object 89223

Number	Time	Miss D (m)	Radial Miss (m)	Obj Xing wrt T	OCO2 Xing wrt T	Xings Rac Diff	Obj AOL	OCO2 AOL	Xing Lat	RA Diff
1	7:17:27.8	1059	336	1.1 later	1.1 earlier	342	274.45	264.54	-80.18	6.824
2	8:56:20.2	940	110	1.0 later	1.0 earlier	105	274.57	264.44	-80.12	6.684
3	10:35:10.6	635	179	0.5 later	0.5 earlier	176	274.70	264.33	-80.08	6.544
4	12:14:01.8	750	313	0.1 later	0.0	313	274.82	264.22	-80.03	6.404
5	13:52:53.0	830	392	0.1 earlier	0.2 later	393	274.95	264.12	-79.98	6.263
6	15:31:44.2	747	455	0.0	0.1 later	455	275.08	264.01	-79.91	6.123
7	17:10:35.5	644	311	0.6 later	0.6 earlier	315	275.21	263.91	-79.83	5.984
8	18:49:26.8	926	159	1.2 later	1.2 earlier	166	275.33	263.80	-79.75	5.843
9	20:28:18.2	1541	298	2.0 later	2.0 earlier	288	275.46	263.70	-79.65	5.700
10	22:07:09.6	1858	321	2.5 later	2.5 earlier	308	275.59	263.59	-79.57	5.559
11	23:46:00.9	1911	231	2.7 later	2.7 earlier	218	275.71	263.49	-79.50	5.419
12	1:24:52.2	2302	130	3.1 later	3.2 earlier	146	275.84	263.38	-79.41	5.280
13	3:03:43.4	2626	23	3.9 later	3.9 earlier	42	275.97	263.28	-79.32	5.141

One approach, similar to what is discussed in [6], is to consider the crossings in a relative sense. This is similar to theory of the 3-D approach when the collision does not have to happen at the prescribed TCA. So if the time of the primary crossing the secondary orbit plane is t_P then the uncertainty of interest is along-track position of the secondary at t_P. A nominal separation time between t_P and the time the secondary crosses the primary orbit plane, t_S

would still be involved. But a one dimensional test then could test the probability that $|t_P - t_S|$ corresponds to a time the tiny time difference corresponding to the two objects being apart by a distance less than the HBR. The one caveat is that the uncertainty of the secondary needs to be the relative uncertainty and thus still contain the uncertainties of both primary and secondary. If they were independent the two covariances could be added. This might serve as a first approximation; however, this is the most likely place that atmospheric drag will affect both quantities so the combined uncertainty would have to be derived accordingly.

3. UPDATE OF Pc FORECASTING TOOL

Version 2 of the PC4 (Raytheon proprietary tool that was introduced in the previous two paper [1,2] included a modification so the current covariance did not have its principal axis necessarily lined up in the miss distance direction in the conjunction plane. However, while implementing this change it was apparent that first figure of [2] (and the corresponding discussion and the poster that was presented) did not match what was coded in Version 1 of PC4. In particular, the way the program works the orientation of the future covariance ellipses is assumed to be the same as the current ellipses. Fig. 3 below illustrates what is actually occurring in Version 1 of PC4. Fig. 4 illustrates the new capability in Version 2 with the miss distance to the Secondary (S) in an arbitrary direction with respect to the covariance ellipses, though again the future covariance is assumed to oriented in the same direction as the current covariance. The grid pattern representing the points of the full-factorial possible position of the future Primary (P2) has been removed for clarity (the grid is discussed in the Monte Carlo section below).

In both versions, assuming the future covariance is oriented the same as the current covariance is likely the best choice. Alternatively, a set of future possible orientations could be considered, however a heuristic argument could be made that assuming the future orientation is the same as the current is not only the most likely situation but also possibly the average of all possible future orientations. Additionally, it should be kept in mind that the conclusion reached in [2] was that the forecasting was only useful for operational staffing. The following describes a more specific example of how the tool can be used for operational decisions.

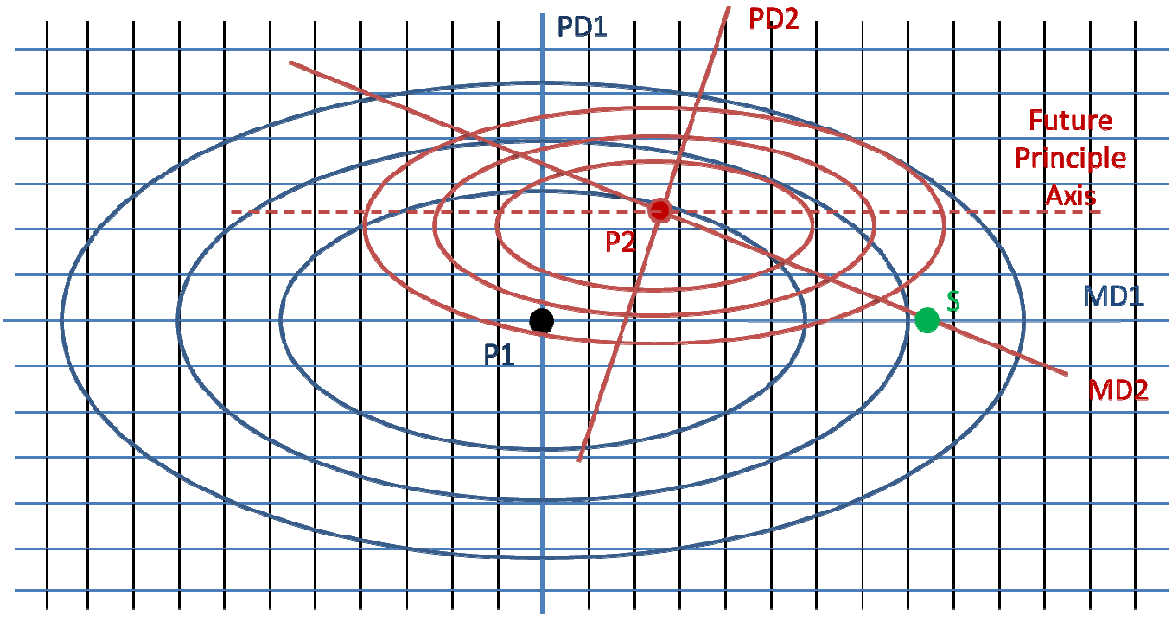

Fig. 3. Geometry of the Covariances/Probability Distributions in Version 1 of the PC4 Tool

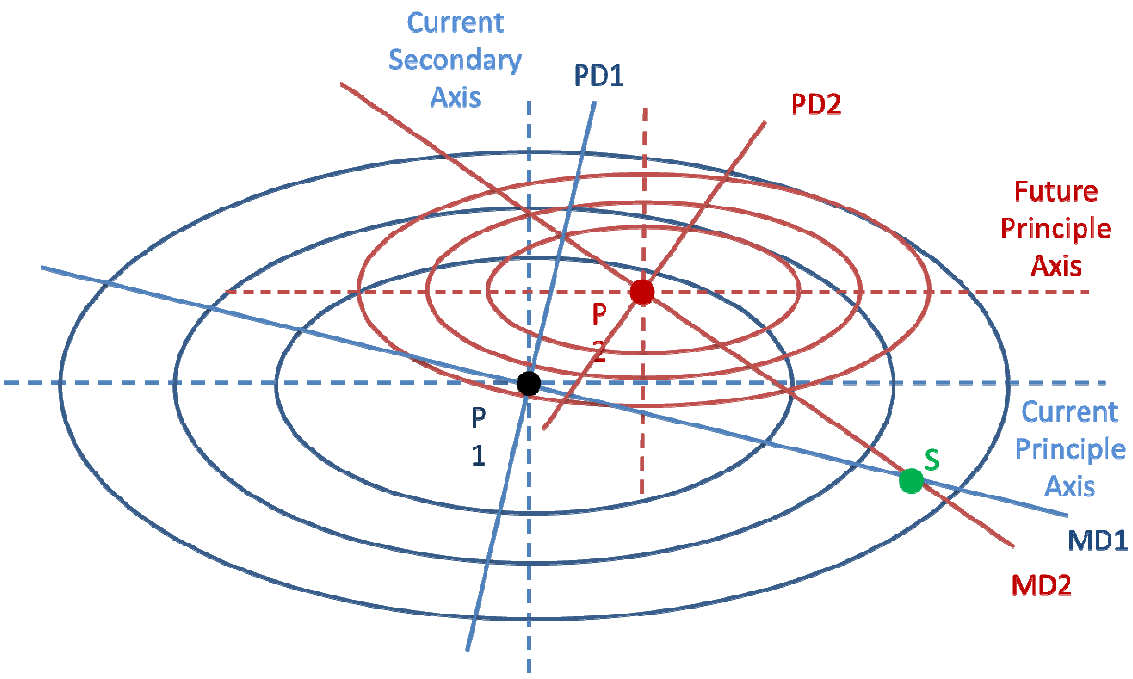

Fig. 4. Geometry of the Covariances/Probability Distributions in Version 2 of the PC4 Tool

As presented in both [1] and [2], the maneuver thresholds for the OCO-2 mission are $1x10^{-5}$ for planning the RMM and $1x10^{-4}$ for its execution. These thresholds have resulted in a lot of planning but few executions since they were adopted. Thus it seemed prudent to investigate whether the planning threshold could be relaxed. The following philosophy was adopted. By delaying the start of the maneuver planning there is a risk that the next solution with new tracking will push the Pc above $1x10^{-4}$ and then an RMM would have to be planned perhaps in an accelerated fashion and/or during non-standard work hours (e.g. in the middle of the night). However, this would be traded for all the cases that the new tracking (or no new tracking) never caused the $1x10^{-4}$ to be exceeded. OCO-2 management agreed that 10% was an acceptable rate for having to do the accelerated process. PC4 was used to find the planning threshold corresponding to this 90/10 success/failure rate.

The preliminary analysis assumed a zero miss distance, attempting to look at the "worst case." As explained below, this over-simplified the problem. Nevertheless, the zero miss results were interesting in themselves. Another assumption made throughout the analyses was that the principle axis of the covariance ellipses was lined up in the miss distance direction and the dimension of the ellipse in that direction was ten times the dimension in the other axes. As discussed in the second chapter of [21] this is a typical combined covariance shape for near circular orbits with an obtuse crossing angle. With these assumptions, the principle axis one-sigma values are given in the corresponding zero miss distance lines in Table 1a assuming the OCO-2 hard body radius of 6 m. PC4 was then run for a series of future covariances, with the same shape but smaller dimensions. Looking at the worst-case future values, the confidence that the Pc would exceed $1x10^{-4}$ with these values only decreased from about 96.5% when starting with an initial Pc of $1x10^{-5}$ to 93% when starting with a Pc of $2x10^{-5}$. However, with an initial Pc of $3x10^{-5}$ the confidence dropped to about 89.5%. Again, these zero miss results were superseded by the non-zero miss results, but they did give an indication of the outcome.

For the non-zero miss the same assumptions were used, however the first realization is that there can be two (10:1 shaped) covariances that match the initial Pc value for a given miss distance. This can be thought of as being on the left or right side of the curves made famous by Alfano [22]. On the right-hand side of Fig. 5 the covariance is large and the Pc values are relatively low. Moving to the left (corresponding to decreasing covariance) the Pc increases to a maximum and then decreases rapidly (except for the zero miss curve).

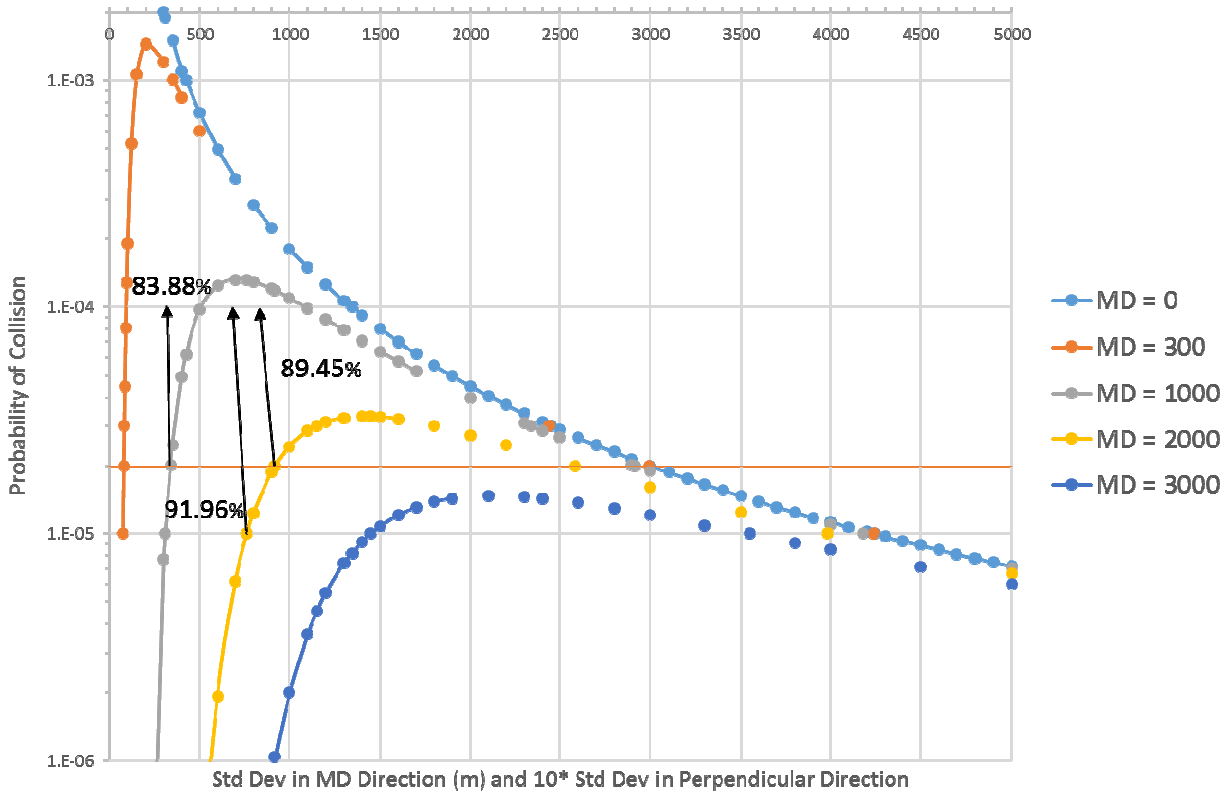

Fig. 5. Confidence Levels of Future Pc Not Jumping to > $1x10^{-4}$

Table 2a. Standard Deviation (m) on Principle Axis for Bigger Covariance side of Curve

Miss D (m)	Pc_1 = 1e-4	Pc_1 = 1e-5	Pc_1 = 2e-5	Pc_1 = 3e-5
0	1342	4243	3000	2449
300	1324	4237	2992	2440
1000	1084	4182	2913	2340
2000	N/A	3983	2582	1797
3000	N/A	3548	N/A	N/A

Table 2b. Standard Deviation (m) on Principle Axis for Smaller Covariance side of Curve

Miss D (m)	Pc_1 = 1e-4	Pc_1 = 1e-5	Pc_1 = 2e-5	Pc_1 = 3e-5
0	N/A	N/A	N/A	N/A
300	92.2	75.1	79.1	81.8
1000	507	309	339	362
2000	N/A	764	920	1151
3000	N/A	1446	N/A	N/A

The first step again was to find the principle axis one-sigma values (σ_{PA}), with the secondary axis value being 1/10 of them, for each Pc value of interest. Table 2a gives these values for the bigger (B) covariance (right-hand) side of the curves in Fig. 5, while Table 2b gives the values for the smaller (S) covariances (left-hand) side of Fig. 4 (again

with the OCO-2 value of 6 m for the hard body radius). Note the first column of Pc = $1x10^{-4}$ values is really just for comparison, since the *current* Pc values of interest are the other three columns. PC4 was then run with representative future principle axis one-sigma values of 800, 700 and 300 m to find the confidence that the corresponding *future* Pc values would not exceed $1x10^{-4}$. The corresponding percent confidence values are presented in Tables 3a, 3b and 3c respectively (continuing the "B" and "S" convention). Note that in all five tables N/A stands for Not Applicable, either because a curve never reaches a Pc value or the assumption that the covariance from the future measurement is smaller than the current value. As mentioned in [2], exceptions to this latter assumption can occur from a future solar storm or a satellite maneuver being performed.

Table 3a. Percent confidence of not exceeding $1x10^{-4}$ when Future σ_{PA} = 800 m

MD	1e-5 B	1e-5 S	2e-5 B	2e-5 S	3e-5 B	3e-5 S
0	96.39	N/A	92.79	N/A	89.55	N/A
300	96.40	N/A	92.81	N/A	89.53	N/A
1000	96.42	N/A	92.86	N/A	89.49	N/A
2000	96.36	N/A	92.90	89.45	89.41	87.85
3000	96.38	95.71	N/A	N/A	N/A	N/A

Table 3b. Percent confidence of not exceeding $1x10^{-4}$ when Future σ_{PA} = 700 m

MD	1x10-5 B	1x10-5 S	2x10-5 B	2x10-5 S	3x10-5 B	3x10-5 S
0	96.56	N/A	93.09	N/A	89.91	N/A
300	96.47	N/A	93.34	N/A	89.94	N/A
1000	96.48	N/A	93.18	N/A	89.95	N/A
2000	96.58	91.96	93.1	89.91	89.77	88.39
3000	96.49	95.89	N/A	N/A	N/A	N/A

Table 3c. Percent confidence of not exceeding $1x10^{-4}$ when Future σ_{PA} = 300 m

MD	1x10-5 B	1x10-5 S	2x10-5 B	2x10-5 S	3x10-5 B	3x10-5 S
0	98.73	N/A	97.02	N/A	95.57	N/A
300	98.50	N/A	97.09	N/A	95.58	N/A
1000	98.53	85.19	97.01	83.88	95.65	82.93
2000	98.55	97.66	97.06	96.37	95.58	95.32
3000	98.48	98.38	N/A	N/A	N/A	N/A

The values in the tables that are red correspond to the arrows in Fig. 4. Starting with a miss distance of 2000 m and a Pc = $2x10^{-5}$ and going to σ_{PA} = 800 m had a confidence level of 89.45%, so just barely breaking the 90% success rate described above. Going down to $1x10^{-5}$ satisfied this criterion for this case, as exemplified by the σ_{PA} = 700 m example. However, when considering a miss distance of 1000 m and σ_{PA} = 300 m, a starting Pc of $2x10^{-5}$ had a low confidence (83.88%) which was not close to satisfying the success criterion. This was enough to come to the following new threshold rule for OCO-2.

Maneuver planning does not have to start until the Pc crosses $2x10^{-5}$ with the caveat that the covariance/miss distance correspond to being on the bigger side of the curve. However, maneuver planning cannot stop until the Pc has dropped down below $1x10^{-5}$. Therefore, all the operational efficiency that was hoped for was not achieved, but a marginal improvement was obtained and has already helped to some extent.

4. MONTE CARLO AND OTHER TECHNIQUES

Monte Carlo (MC) simulations are often referred to as the "gold standard" for comparisons to other methods, such as polynomial chaos [23]. Although these are valid comparisons, arguably the full factorial (FF) method is more of a standard. Of course, FF suffers even more from the "curse of dimensionality" and the precision of its results are a function of the bin size used to represent the input variables. The usefulness of the MC is that its computational efficiency still allows analysis to be done when the FF method corresponds to intractable computer run times. Nevertheless, it should be kept in mind that the MC is a random approximation of the desired answer.

As a side note, there are (at least) two different methods to implement a FF analysis. Commonly the cells of input data are chosen to have equal probability, that is a greater density of cells near the peaks of the probability distribution functions and less dense near their tails. However, as evident in the equally spaced pattern in Fig. 2, the PC4 tool had equally spaced values in the two input variables chosen at the center of each grid cell. This implies that each cell had an individual probability weight (of course with symmetry reflected across each center line). It was easier to code in this manner and then choose a large number (200) of cells to achieve enough precision, rather than having cells having equal probability which is computationally more efficient but more difficult to code.

To illustrate how a better understanding of how the results of MC can be interpreted in the context of Pc calculations consider the "Wilson Interval" [24]. It is a confidence interval around a MC result. For this example, the number of MC trials (aka "draws") that are needed to have a 99% confidence that the Pc < 1×10^{-4} (the maneuver threshold mentioned above) is obtained. Let n be the number of trials that are needed. A 99% confidence corresponds to a target error rate $\alpha = 0.01$, so for this two-sides test $1 - \alpha/2 = 0.995$ which, from a standard normal distribution table gives the desired quantile $z = 2.576$. For this example, consider the case where one trial results in a collision between the two objects. The quantity p represents the proportion of "hits" with respect to the number of trials, so for this example 1/n. The Wilson Interval is:

$$\frac{1}{\left(1+\frac{z^2}{n}\right)}\left[p+\frac{z^2}{2n}+z\sqrt{\frac{p(1-p)}{n}+\frac{z^2}{4n^2}}\right] \tag{8}$$

Using a spreadsheet to iterate on the number n, a value of n = 85178 gave the 99% confidence interval to be 5.06886 x 10^{-5} +/- 4.93104 x10^{-5}, corresponding to a maximum limit of 9.9999 x10^{-5}. Note one less trial (85177) gave a maximum value slightly above 1×10^{-4}. Thus if one collision occurs then at least 85178 trials need to have been used to have the 99% confidence that the Pc < 1×10^{-4}. Perhaps even more surprisingly, note that even with no collision results (p=0) and a much simplified formula, n must be 66,352 trials for the same upper limit (though care must be taken in interpreting results when p is exactly zero). For example, the Wald test, which treats the distributions in the tails as binomial ones, is not valid when p = 0. In summary, the number of MC trials needed for confidence in a result may be much more than an analyst might expect.

Finally, since the use of MC is for computational efficiency, it should be mentioned that sample-based methods such as the aforementioned polynomial chaos theory, increase the efficiency even more. An alternative method, named the Trinomial Method [25] was created to only look at the tails of the distributions. It was developed for the orbit lifetime prediction portion of the Mars orbiter planetary protection process. However, any application to the Pc calculation process is still under investigation.

5. CONCLUSIONS

The investigation into the use of equinoctial elements in the end-to-end process of determining Pc provided interesting insight into the uncertainties involved. A new two-step process, a spatial test involving 5 elements and temporal test involving the 6th (and fast) element was developed at the preliminary level. Future analysis will test to see if this method lowers the Pc value and/or eases the computational burden. Another future possibility is to include the correlations between the elements of the two objects involved in the conjunction. A new application of the PC4 forecasting tool was discovered. Finally, cautions must be exercised when using Monte Carlo results as a standard.

6. ACKNOWLEDGEMENTS

Funding was provided by the OCO-2 Project of the Jet Propulsion Laboratory/California Institute of Technology.

7. REFERENCES

1. Vincent, M.A., Bridging the gap between academia and operations for orbital debris risk mitigation, Proc. Of the Advanced Maui Optical and Space Surveillance Technologies Conference, Sept. 15-18, 2015.
2. Vincent, M.A., Paving the bridge between academia and operations for orbital debris risk mitigation, Proc. Of the Advanced Maui Optical and Space Surveillance Technologies Conference, Sept. 20-23, 2016.
3. Sabol, C., Sukurt, T., Hill, K., Alfriend, K.T., Wright, B., Li, Y., Schumacher, P., Linearized Orbit Covariance Generation and Propagation Analysis via Simple Monte Carlo Simulations, *Advances in Astronautical Science* Vol 134, 2010.
4. Vincent, M.A., The Geometry of Repeating Conjunctions, Proc. of the Space Situational Awareness Operators' Workshop, Denver, CO, November 3-5, 2016.
5. Hoots, F.R., Crawford, L.L., Roerich, R.L., An Analytic Method to Determine Future Close Approaches between Satellites, *Celestial Mechanics*, Vol 33, 1984.
6. Woodburn, J., Coppola, V., Stoner, F., A Description of Filters for Minimizing the Time Required for Orbit Conjunction Computations, *Advances in Astronautical Sciences* Vol 372, 2009.
7. Roy, A.E., *Orbital Motion*, Halsted Press, 1978.
8. Vallado, D.A., *Fundamentals of Astrodynamics and Applications*, 4th Edition, Microcosm Press, 2013.
9. Wiesel, W.E., A KAM Tori Algorithm for Earth Satellite Orbits, under review by the *Journal of Astronautical Sciences*
10. Sweetser, T.H., Vincent, M.A., The Eccentric Behavior of Nearly Frozen Orbits, Proc. of AAS/AIAA Astrodynamics Specialist Conference, Hilton Head, South Carolina, August 11-15, 2013.
11. Vincent, M.A., Reconfiguring the A-Train and Shrinking the Earth Science Constellations' Envelope, Proc. Of the 9th International Workshop on Satellite Constellations and Formation Flying, Paper 63, June 19-21, 2017.
12. Setty S.J., Cefola, P.J., Fielder, H., Diaz, J.F.S.J., Attributes affecting the Accuracy of a Batch Least Squares Orbit Determination using Semi-analytical Satellite Theory, Proc. of the Maui Optical and Space Surveillance Technologies Conference, Sept. 20-23, 2016.
13. Cefola, P.J., Sabol, C., Hill, K., Nishimoto, D., Demonstration of the DSST State Transition Matrix Time-update Properties using the LINUX GTDS Program, Proc. of the Maui Optical and Space Surveillance Technologies Conference, Sept. 13-16, 2011.
14. Smith, J.C., Planetary Observer Planning Software (POPS), Reference JPL-45418, NASA Technology Transfer Program, also JPL Internal Document EM 312/91-162, February, 1991.
15. Guinn, J.R., Periodic Gravitational Perturbations for Conversion between Osculating and Mean Orbit Elements, *Advances in Astronautical Sciences*, Vol. 76, Specialist Conference, Durango, CO August 19-22, 1991.
16. Kaula W.M., *Theory of Satellite Geodesy*, Dover Publications 2000.
17. Ely, T.A., Transforming Mean and Osculating Elements using Numerical Methods, Journal of Astronautical Sciences, Vol. 62.1, March 2015.
18. Ely, T.A., Mean Element Propagations using Numerical Averaging, *Journal of Astronautical Sciences*, Vol. 61.3, 2014.
19. Alfriend, K.T., Park. I., When does the Uncertainty become Non-Gaussian, Proc. Of the Advanced Maui Optical and Space Surveillance Technologies Conference, Sept. 20-23, 2016.
20. Horwood, J.T., Singh, N., Aristoff, J.M., Bhopale, A., KRATOS: Kollision Risk Assessment Tool in Orbital Element Space, Proc. Of the Advanced Maui Optical and Space Surveillance Technologies Conference, Sept. 20-23, 2016.
21. Chan F.K., *Spacecraft Collision Probability*, The Aerospace Press, 2008.
22. Alfano S, "Relating Position Uncertainty to Maximum Conjunction Probability," *Journal of Astronautical Sciences* Vol. 53, No.2, 2005.
23. Jones, B.A., Doostan, A., Satellite Collision Probability Estimation using Polynomial Chaos Expansion, Advances in Space Research, Vol. 52, August, 2013.
24. Wilson, E.B., Probable inference, the law of succession, and statistical inference, *Journal of the American Statistical Association*, Vol. 22, 209-212, 1927.
25. Vincent, M.A., A New Method of Determining Orbit Lifetime Probabilities for Use in Planetary Protection, AAS 97-736 Proc. of the AAS/AIAA Astrodynamics Specialist Conference, Sun Valley, ID, August 4-7, 1997.